AIAA 94-0064

Sensitivity Analysis of Unsteady Aerodynamic Loads in Cascades

C. B. Lorence and K. C. Hall
Duke University
Durham, NC

32nd Aerospace Sciences Meeting & Exhibit
January 10-13, 1994 / Reno, NV

SENSITIVITY ANALYSIS OF UNSTEADY AERODYNAMIC LOADS IN CASCADES

Christopher B. Lorence* and Kenneth C. Hall†
Duke University
Durham, NC 27708-0300

Abstract

A method for computing the effect perturbations in the shape of airfoils in a cascade have on the steady and unsteady flow through the cascade is presented. First, the full potential equation is used to describe the behavior of the nonlinear mean (steady) flow and the small disturbance unsteady flow through the cascade. The steady flow and small disturbance unsteady flow versions of the full potential equation are then discretized using quadrilateral isoparametric finite elements. The nonlinear mean flow solution is computed using Newton iteration. At each step of the Newton iteration, LU decomposition is used to solve the resulting set of linear equations. The unsteady flow problem is linear, and is also solved using LU decomposition. Next, a sensitivity analysis is performed to determine the effect small changes in cascade and airfoil geometry have on the mean and unsteady flow fields. The sensitivity analysis makes use of the nominal steady and unsteady flow LU decompositions so that no additional matrices need to be factored. Hence, the present method is computationally very efficient. Finally, we demonstrate how the sensitivity analysis may be used to redesign cascades for improved aeroelastic stability.

Introduction

As the efficiency of modern aircraft engines continues to increase, aeroacoustic and aeroelastic considerations play an increasingly important role in the design of turbomachinery blading. Government regulations and community standards demand reduced levels of noise from aircraft, while competitive pressures require increased efficiency and mechanical reliability. Currently, however, the steady aerodynamic design and the aeroelastic design phases during the development of compressor, and turbine blading are largely decoupled. First, the blade is designed primarily to maximize steady aerodynamic performance. Then, detailed aeroelastic studies are performed to determine whether the blades will meet standards for flutter stability and fatigue. If the blade fails to meet these requirements, the blade is redesigned, and the process is repeated. This redesign process increases the time and expense required to design a blade and misses an opportunity to simultaneously design for steady and unsteady aerodynamic performance.

In recent years, the capability to analyze unsteady flows in cascades has substantially improved. For example, a number of linearized analyses of unsteady flows about loaded airfoils have been developed. These include potential analyses [1, 2], potential analyses with vortical gust effects [3, 4], and linearized Euler analyses [5, 6, 7, 8]. Although these models were developed primarily for use in aeroelastic analyses, they are also well suited for modeling the aeroacoustic response of cascades to vortical gusts and potential interaction arising from nearby blade rows. These linearized flow models are best viewed as *analysis* tools rather than design tools. They are capable of solving the direct problem where the shape of the airfoil as well as the flow conditions are specified. Unfortunately, except through trial and error or extensive parametric studies, these codes do not provide physical insight into how, for example, to design cascades to be aeroelastically stable or to minimize the acoustic response due to wake interaction.

A substantial body of work exists on the inverse design and optimal design of airfoils. Most of this work, however, is directed at achieving desirable *steady* flow properties. For example, Lighthill [9] developed an inverse design method based on conformal mapping techniques. More recently, a number of investigators have proposed inverse design techniques based on modern computational fluid dynamic algorithms (e.g., [10]). A number of investigators have used nonlinear programming techniques (e.g., [11]), and Jameson has suggested that the airfoil design problem may be viewed as an optimal control problem [12]. Researchers have also developed aeroelastic optimization techniques for rotorcraft [13], aircraft [14], and turbomachinery [15]. These analyses, however, have focused on structural optimization rather than optimization of the unsteady aerodynamic behavior.

One of the key ingredients in optimization algorithms is the evaluation of the sensitivity of the quantity to be optimized (for example, the flutter stability or efficiency of a cascade) to a small change in a physical parameter (such as the airfoil shape). Sensitivity analysis of structures has been an active area of research for the past decade [16, 17]. Recently, researchers have begun to develop similar sensitivity analysis techniques for steady aerodynamic problems. For example, Taylor *et*

*Graduate Research Assistant, Department of Mechanical Engineering and Materials Science, Member AIAA.
†Assistant Professor, Department of Mechanical Engineering and Materials Science, Member AIAA.

al [18] and Baysal and Eleshaky [19] have computed the effect of modifying the shape of a nozzle on the flow in the nozzle. Their work was based on a sensitivity analysis of the discretized Euler equations. Most recently, such techniques have been applied to airfoil design [20]. Despite these advances, only a few unsteady sensitivity analyses have been reported in the literature – for example the semi-analytical panel method of Murthy and Kaza [21]. Other unsteady aerodynamic sensitivity analyses have been performed by numerically differencing two unsteady flow solutions computed for slightly different values of some physical parameter. The use of finite difference sensitivity analyses, however, is less desirable than an analytical method because of the large computational expense and susceptibility to round-off and truncation errors associated with finite difference techniques.

In this paper, we present a new method for computing the sensitivity of steady and unsteady flows in cascades to small changes in airfoil and cascade geometry. The nominal steady and unsteady flows are computed using a full potential solver based on a deforming grid variational principle and finite element method developed by Hall [22]. To calculate the sensitivities, a perturbation analysis is performed on the nominal steady and unsteady finite element equations. This leads to a set of linear matrix equations for the sensitivity of the steady and unsteady potential due to small changes in the airfoil shape. The matrix equations to be solved are the same as the nominal flow matrix equations, but with new right-hand sides. Thus, if the nominal flows have been computed using LU decomposition, then no additional matrices need to be factored, and the sensitivities can be computed by back-substitution. Consequently, the sensitivity of the steady and unsteady potentials can be computed very efficiently. The approach is general in nature and can be applied to different governing equations and numerical schemes.

Theory

Nominal Flow Field Description

In the present analysis, the flow through a blade row is assumed to be inviscid, isentropic, irrotational, and two-dimensional. In addition, the fluid is assumed to be an ideal gas with constant specific heats. Thus, the velocity field can be represented by the gradient of a scalar potential, $\hat{\phi}$. This potential satisfies the unsteady full potential equation

$$\nabla^2\hat{\phi} = \frac{1}{\hat{c}^2}\left[\frac{\partial^2\hat{\phi}}{\partial t^2} + 2\nabla\hat{\phi}\cdot\nabla\frac{\partial\hat{\phi}}{\partial t} + \frac{1}{2}\nabla\hat{\phi}\cdot\nabla\left(\nabla\hat{\phi}\right)^2\right] \quad (1)$$

where $\hat{c}$ is the local speed of sound. The static density and pressure may be expressed in terms of the velocity potential as

$$\hat{\rho} = \rho_T\left\{1 - \frac{\gamma-1}{C_T^2}\left[\frac{1}{2}(\nabla\hat{\phi})^2 + \frac{\partial\hat{\phi}}{\partial t}\right]\right\}^{\frac{1}{\gamma-1}} \quad (2)$$

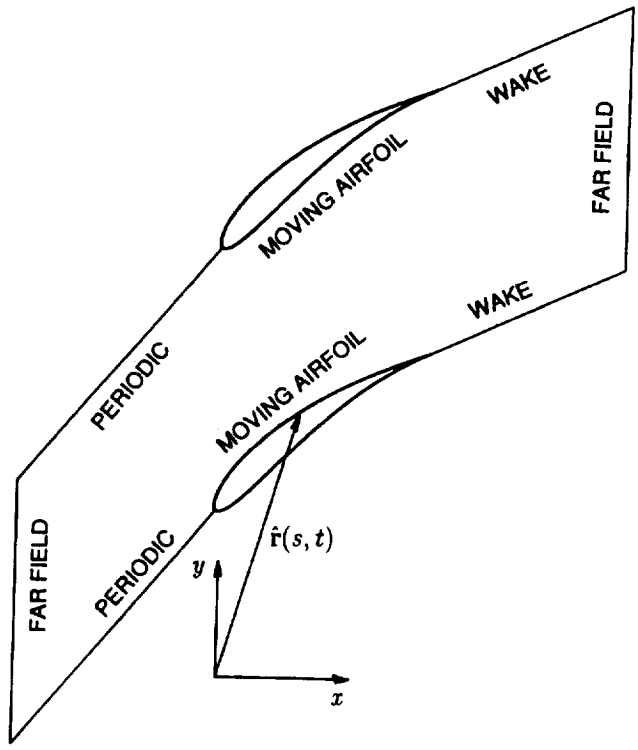

Figure 1: Typical solution domain used for calculation of flow through cascades. Five main boundary types are moving airfoil, upstream periodic, downstream wake, upstream far field, and downstream far field.

$$\hat{p} = p_T\left\{1 - \frac{\gamma-1}{C_T^2}\left[\frac{1}{2}(\nabla\hat{\phi})^2 + \frac{\partial\hat{\phi}}{\partial t}\right]\right\}^{\frac{\gamma}{\gamma-1}} \quad (3)$$

where ρ_T and p_T are the total density and total pressure, respectively, and C_T is the total speed of sound. Equation (3) is simply the unsteady Bernoulli equation.

To complete the problem specification, boundary conditions must be specified (see Fig. 1). On airfoil surfaces, the boundary condition is that there can be no mass flux through the airfoil so that

$$\nabla\hat{\phi}\cdot\hat{\mathbf{n}} = \frac{\partial\hat{\mathbf{r}}}{\partial t}\cdot\hat{\mathbf{n}} \quad (4)$$

where $\hat{\mathbf{n}}$ is the unit normal to the airfoil surface, and the surface of the airfoil at any time t is described by the parameterized position vector $\hat{\mathbf{r}}$. The wake is considered to be an impermeable surface so that Eq. (4) also applies on both sides of the wake. Also, the pressure must be constant across the wake so that

$$[\![\hat{p}]\!] = 0 \quad (5)$$

where $[\![\hat{p}]\!]$ is the pressure jump across the wake. Periodic boundary conditions are applied along the upstream and downstream periodic boundaries to reduce

the computational domain to a single blade passage. Finally, for unsteady flow problems, nonreflecting boundary conditions must be applied on the upstream and downstream far-field boundaries to prevent spurious reflections of outgoing waves.

The problem of solving for the unsteady flow in the cascade is divided into two parts. First, we solve for the nonlinear steady or mean flow through the cascade. Next, we assume that the unsteadiness in the flow is a small harmonic disturbance about the mean flow with frequency ω. Therefore, the unsteady perturbation flow is described by a set of linear variable coefficient equations.

To increase the accuracy of the unsteady solution procedure, the unsteady velocity potential is computed on a deforming computational grid which conforms to the motion of the moving airfoils. We define two coordinate systems. The first coordinate system (x, y, t) is the usual inertial coordinate system. The second coordinate system (ξ, η, τ) is the computational coordinate system which is attached to the computational grid. Thus a point fixed in the computational coordinate system (ξ, η, τ) moves in the physical coordinate system (x, y, t) as the grid deforms. Because the motion of airfoils (and hence the grid) is small, the two coordinate systems differ by a small perturbation, i.e.,

$$x(\xi, \eta, \tau) = \xi + f(\xi, \eta)e^{j\omega\tau} \tag{6}$$

$$y(\xi, \eta, \tau) = \eta + g(\xi, \eta)e^{j\omega\tau} \tag{7}$$

$$t(\xi, \eta, \tau) = \tau \tag{8}$$

where f and g are the complex amplitudes of the small perturbation. Note that to zeroth order, the physical and computational coordinate systems are identical.

Similarly, the velocity potential is expanded in a perturbation series

$$\hat{\phi}(\xi, \eta, \tau) = \Phi(\xi, \eta) + \phi(\xi, \eta)e^{j\omega\tau} \tag{9}$$

where Φ and ϕ are the mean flow and small disturbance unsteady velocity potentials, respectively. Substitution of Eqs. (6)-(9) into the full potential equation, Eq. (1), and collection of terms of zeroth and first order gives the mean flow and small disturbance flow equations. The mean flow potential equation is given by

$$\nabla^2\Phi = \frac{1}{C^2}\left[\frac{1}{2}\nabla\Phi \cdot \nabla\left(\nabla\Phi\right)^2\right] \tag{10}$$

where C is the speed of sound, and is a function of the potential Φ. Note that Eq. (10) is nonlinear in the unknown potential Φ. The small disturbance unsteady potential equation is given by

$$\nabla' \cdot R\nabla'\phi - \nabla' \cdot \left[\frac{R}{C^2}\left(\nabla'\Phi^T\nabla'\phi + j\omega\phi\right)\nabla'\Phi\right]$$

$$- \frac{R}{C^2}\left(j\omega\nabla'\Phi^T\nabla'\phi - \omega^2\phi\right) = b \tag{11}$$

where b is an inhomogeneous term that is a function of the computed steady flow and the prescribed grid motion (see [22]), and R is the mean flow density. Here ∇' is the gradient in the (ξ, η) coordinate system, i.e., $\nabla = \mathbf{J}\nabla'$, where $\mathbf{J}$ is the Jacobian of the coordinate transformation. The small disturbance equation is seen to be linear in the unsteady potential, ϕ, with coefficients that depend on the nonlinear steady flow potential, Φ.

In a completely analogous fashion, the boundary conditions may be split into mean flow and small disturbance flow parts. For example, the no through flow condition on the airfoil, Eq. (4), becomes

$$\frac{\partial\Phi}{\partial n} = 0 \tag{12}$$

for the steady flow problem, and

$$\frac{\partial\phi}{\partial n} = j\omega\mathbf{f} \cdot \bar{\mathbf{n}} - \tilde{\mathbf{J}}\nabla'\Phi \cdot \bar{\mathbf{n}} \tag{13}$$

for the small disturbance flow problem. In Eq. (13), $\tilde{\mathbf{J}} = \mathbf{J}^T\mathbf{J} - \mathbf{I}$, and $\mathbf{f}$ is the vector of grid motion functions, $(f, g)^T$. The first term of the right-hand side of Eq. (13) represents the upwash due to translation of the airfoil. The second term is an additional upwash due to the shearing of the steady potential field near the airfoil surface. The usual upwash term arising from the rotation of the airfoil surface, as well as the extrapolation term encountered in fixed grid computations, do not appear because we perturb the velocity potential in the coordinate system attached to the deforming grid.

In addition, mean flow and small disturbance flow boundary conditions must be specified at the inflow, outflow, periodic, and wake boundaries (see Fig. 1). For brevity, we omit the details of these boundary conditions. The far-field boundary conditions for the unsteady flow solver are analytically exact nonreflecting boundary conditions based on the behavior of the linearized full potential equation in the far-field [23]. The remaining boundary conditions are substantially the same as in Ref. [22].

Once one has solved for the mean and small disturbance potentials, one can compute the resulting steady pressure P and unsteady pressure p using the Bernoulli equation. Expanding Eq. (3) in a perturbation series gives

$$P = p_T\left\{1 - \frac{\gamma - 1}{2C_T^2}(\nabla\Phi)^2\right\}^{\frac{\gamma}{\gamma-1}} \tag{14}$$

and

$$p = -R\left[\nabla'\Phi^T\nabla'\phi + j\omega\phi - j\omega\mathbf{f} \cdot \nabla'\Phi + \frac{1}{2}\nabla'\Phi^T\tilde{\mathbf{J}}\nabla'\Phi\right] \tag{15}$$

Note in particular that the unsteady pressure p is produced by the small disturbance potential ϕ, and by the deformation of the steady potential field Φ. Finally, appropriate integrations of the pressure around the airfoil give the steady and unsteady lift and moment acting on the airfoils.

Numerical Solution Technique

One could solve the above differential equations in a number of ways, e.g., using finite difference, finite volume, or finite element techniques. In the present analysis, we discretize these equations using a variational finite element technique. Hall [22] has shown that Eqs. (10) and (11) are the Euler-Lagrange equations of steady flow and small disturbance unsteady flow variational principles based on a variational principle due to Bateman [24]. Furthermore, the natural boundary condition of the variational principles are the steady and small disturbance no through flow conditions, Eqs. (12) and (13), respectively.

First, consider the solution of the steady flow problem. The steady flow variational principle is discretized using quadrilateral isoparametric finite elements. The auxiliary boundary conditions are discretized using a combination of finite element and finite difference techniques. The result is a set of nonlinear equations of the form

$$\mathbf{N}(\mathbf{V};\mathbf{X}) = \mathbf{0} \tag{16}$$

where $\mathbf{N}$ is a vector of nonlinear functions, $\mathbf{V}$ is the vector containing the as yet unknown steady velocity potential Φ at each of the computational nodes, and $\mathbf{X}$ is a vector containing the location of the computational nodes (thus the airfoil shape is also contained in $\mathbf{X}$).

To solve Eq. (16) for the nominal airfoil and cascade geometry, we use Newton iteration. Hence, given the nth estimate of the solution $\mathbf{V}^n$, the $(n+1)$st estimate is given by

$$\mathbf{V}^{n+1} = \mathbf{V}^n - \left[\frac{\partial \mathbf{N}}{\partial \mathbf{V}}\right]_n^{-1} \mathbf{N}(\mathbf{V}^n, \mathbf{X}) \tag{17}$$

Using Newton iteration, the system of nonlinear equations, Eq. (16), is reduced to a sequence of linear equations, Eq. (17). Because we use an H-grid in the present investigation, the matrix $\partial\mathbf{N}/\partial\mathbf{V}$ is block tridiagonal. Of course the matrix is not actually inverted, but rather factored using an LU decomposition algorithm which takes advantage of the block-tridiagonal structure. The Newton iteration procedure is very fast with solutions typically obtained in about five iterations.

Having computed the nominal steady solution, we next discretize and solve the nominal linearized unsteady flow problem. The small disturbance variational principle is discretized, again using quadrilateral isoparametric finite elements. The auxiliary equations are discretized using a combination of finite elements and finite difference operators. The result is a linear matrix equation of the form

$$\mathbf{A}\mathbf{v} = \mathbf{b} \tag{18}$$

where

$$\mathbf{A} = \mathbf{A}(\mathbf{V}, \mathbf{X}, \omega)$$
$$\mathbf{b} = \mathbf{b}(\mathbf{V}, \mathbf{X}, \mathbf{f}, \omega)$$

and $\mathbf{v}$ is the vector containing the nodal values of the unsteady velocity potential ϕ. Equation (18) is large, sparse, complex, and block tridiagonal, and is solved efficiently using LU decomposition.

Sensitivity Analysis

Now that the nominal steady and unsteady flow problems have been solved, the next step is to determine the effect a small change in airfoil or cascade geometry has on the steady and unsteady flow. Returning to Eq. (16), if the geometry is perturbed slightly, the perturbed solution will satisfy the equation

$$\mathbf{N}(\mathbf{V}+\mathbf{V}';\mathbf{X}+\mathbf{X}') = \mathbf{0} \tag{19}$$

where $\mathbf{X}$ is the nominal cascade geometry, $\mathbf{X}'$ is the perturbation in the geometry, $\mathbf{V}$ contains the nominal steady velocity potential, and $\mathbf{V}'$ is the sensitivity of the steady potential to perturbations in the geometry. Expanding Eq. (19) in a perturbation series about the nominal solution gives

$$\left[\frac{\partial \mathbf{N}}{\partial \mathbf{V}}\right]\mathbf{V}' + \left[\frac{\partial \mathbf{N}}{\partial \mathbf{X}}\right]\mathbf{X}' = \mathbf{0} \tag{20}$$

Solving for the unknown perturbation $\mathbf{V}'$ gives

$$\mathbf{V}' = -\left[\frac{\partial \mathbf{N}}{\partial \mathbf{V}}\right]^{-1}\left[\frac{\partial \mathbf{N}}{\partial \mathbf{X}}\right]\mathbf{X}' \tag{21}$$

Computationally, $[\partial\mathbf{N}/\partial\mathbf{X}]\mathbf{X}'$ is very inexpensive to form. Furthermore, note the similarity of Eq. (21) to Eq. (17). The same matrix must be "inverted" to obtain the perturbed steady solution that was used in the last iteration of the Newton solver. Therefore, if the steady flow has been computed using Newton iteration with LU decomposition, and the last factored matrix has been saved, then the sensitivity $\mathbf{V}'$ can be obtained with very little additional computational work.

Having computed the sensitivity of the steady potential to a change in geometry, it is now possible to compute the resulting sensitivity of the unsteady potential. The solution of the unsteady flow problem due to small changes in the geometry, frequency, and mode shape will be of the form

$$[\mathbf{A}(\mathbf{V}+\mathbf{V}', \mathbf{X}+\mathbf{X}', \omega+\omega')]\{\mathbf{v}+\mathbf{v}'\} = \mathbf{b}(\mathbf{V}+\mathbf{V}', \mathbf{X}+\mathbf{X}', \mathbf{f}+\mathbf{f}', \omega+\omega') \tag{22}$$

where $\mathbf{f}'$ is the prescribed perturbation in the motion of the airfoil and grid, ω' is the prescribed perturbation in the frequency of the unsteady motion, and $\mathbf{v}'$ is the unknown sensitivity of the unsteady potential. Expanding Eq. (22) in a perturbation series and collecting terms of first order gives the desired equation for the unknown $\mathbf{v}'$,

$$[\mathbf{A}]\mathbf{v}' = \left[\frac{\partial \mathbf{b}}{\partial \mathbf{V}}\right]\mathbf{V}' + \left[\frac{\partial \mathbf{b}}{\partial \mathbf{X}}\right]\mathbf{X}' + \left[\frac{\partial \mathbf{b}}{\partial \mathbf{f}}\right]\mathbf{f}' + \left[\frac{\partial \mathbf{b}}{\partial \omega}\right]\omega' - \left(\left[\frac{\partial \mathbf{A}}{\partial \mathbf{V}}\right]\mathbf{V}' + \left[\frac{\partial \mathbf{A}}{\partial \mathbf{X}}\right]\mathbf{X}' + \left[\frac{\partial \mathbf{A}}{\partial \omega}\right]\omega'\right)\mathbf{v} \tag{23}$$

or more succinctly

$$[\mathbf{A}]\,\mathbf{v}' = \mathbf{b}' - [\mathbf{A}]'\mathbf{v} \tag{24}$$

Note that the terms $\mathbf{X}'$, $\mathbf{f}'$, and ω' are prescribed, and $\mathbf{V}'$ is known from the solution of the steady sensitivity problem.

In principle, one could assemble the matrices $[\partial\mathbf{b}/\partial\mathbf{V}]$, $[\partial\mathbf{A}/\partial\mathbf{V}]$, etc. in Eq. (23), then multiply by the known perturbations and sum the results to obtain the right-hand side of Eq. (23). However, it is computationally much more efficient to perform the multiplications and summations during the integration phase of the finite element construction. Hence, at the element level, we construct $\mathbf{A}'$ and $\mathbf{b}'$ directly without ever forming the derivative terms. The elemental matrix $\mathbf{A}'$ is multiplied by the elemental vector $\mathbf{v}$ and the result subtracted from the elemental vector $\mathbf{b}'$. Finally, the elemental contributions are assembled to form the global right-hand side to Eq. (24).

As in the steady sensitivity analysis, the computational effort required to solve for $\mathbf{v}'$ is insignificant since the matrix $[\mathbf{A}]$ has already been factored into upper and lower triangular matrices when the nominal unsteady solution $\mathbf{v}$ was computed.

Finally, we note that although the present sensitivity analysis has been applied to a finite element discretization of the steady and unsteady full potential equation, the method can be applied equally well to finite difference and finite volume discretizations, and may be applied to other flow models (e.g., Euler, Navier-Stokes) as well. The crucial feature which makes the present sensitivity analysis computationally efficient is the use of LU decomposition in the nominal steady and unsteady flow solvers.

Results

Steady Flow Through a Compressor

To demonstrate the present sensitivity analysis, we will analyze a linear cascade of NACA four digit airfoils. The nominal cascade is similar to modern compressor cascades, and is composed of NACA 5506 airfoils. For the case considered here, the inflow Mach number $M_{-\infty}$ is 0.5, the inflow angle $\beta_{-\infty}$ (measured from the axial direction) is 55°, the stagger angle Θ is 45°, and the blade-to-blade gap G is 0.9. Figure 2 shows the nominal steady surface pressure, P, for two different grid resolutions, a 65×17 node grid and a 129×33 node grid (the pressure has been nondimensionalized by the upstream density times the inflow velocity squared). The flow is entirely subsonic with a maximum Mach number on the suction surface of about 0.61. Note also the good agreement between the coarse grid and fine grid solutions.

Having computed the nominal flow through the cascade, we next consider the effect of six different design parameters on the steady flowfield. Three of these parameters are from the NACA four digit airfoil definition: the airfoil thickness, camber, and position of maximum camber. Each of these quantities are measured in fractions of the airfoil chord c. We also consider the effect of changes in the cascade stagger angle Θ, and blade-to-blade gap G. Finally, we introduce an additional design variable, the reflex. The reflex parameter modifies the height of the mean line by the magnitude of the reflex times the chord c times $\sin(2\pi\xi/c)$, where ξ is the distance along the airfoil chord.

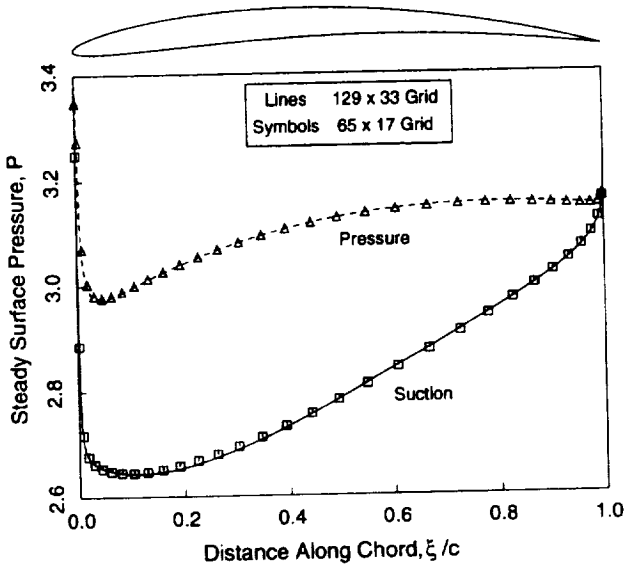

Figure 2: Steady surface pressure of cascade of NACA 5506 airfoils. $M_{-\infty} = 0.5$, $\beta_{-\infty} = 55°$, $\Theta = 45°$.

Figure 3 shows the sensitivity of the steady surface pressure to changes in five of the six geometry variables (the sensitivity to maximum camber location is not shown). The sensitivities are computed using the present sensitivity analysis; all results were computed on a 65×17 node grid. To check these results, we also compute the sensitivities using a finite difference approach. The finite-difference result is computed by solving for the steady flow about two slightly different airfoils, differencing the two, and dividing the result by the difference in the airfoil parameter. Note the excellent agreement between the two solutions indicating that the effect of small changes in the design variables is linear, and that the present sensitivity analysis correctly predicts the sensitivities. Also, one sees that the largest sensitivity in pressure occurs near the leading edge of the airfoil.

Next, the surface pressure sensitivities were integrated to obtain the sensitivity of the steady lift and drag (measured normal to and along the chord) and the moment about the leading edge. These results are given in Table 1. Also tabulated is the sensitivity of the lift in the y-direction (the cascade direction). The steady lift in the y-direction is a measure of the turning done by the cascade and hence is related to the steady

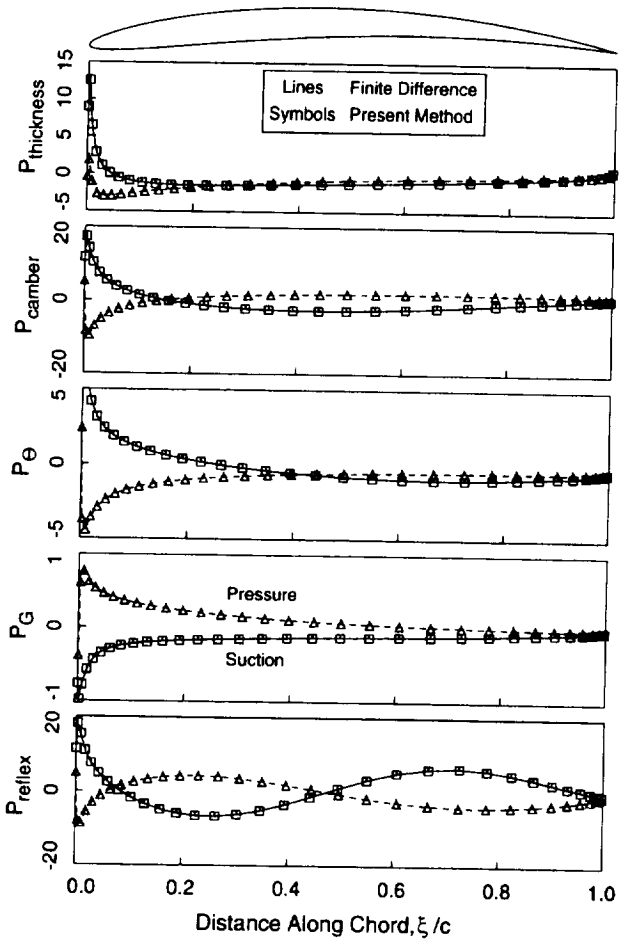

Figure 3: Sensitivity of steady surface pressure of cascade of NACA 5506 airfoils to perturbations in thickness, camber, stagger, gap, and reflex. $M_{-\infty} = 0.5$, $\beta_{-\infty} = 55°$, $\Theta = 45°$.

Table 1: Sensitivity of steady forces and moment. The nominal steady lift, L, is 0.2907, the nominal drag, D, is -0.0177, the nominal moment about the leading edge, M_{LE}, is -0.1215, and the nominal lift in the y-direction, L_Y, is 0.1931.

Variable	L'	D'	M'_{LE}	L'_Y
Thickness	-0.1935	-0.0135	-0.1234	-0.1464
Camber	1.5637	0.1446	-1.4003	1.2080
Stagger	-0.6632	-0.0642	-0.0548	-0.5144
Gap	0.2743	-0.0244	-0.0764	0.1767
Max. C. Loc.	0.0873	0.0083	-0.1060	0.0676
Reflex	-1.5506	-0.1476	1.9235	-1.2008

work done by the cascade. Table 1 shows that the lift in the y-direction is most sensitive to changes in camber, stagger angle, and reflex. Since these parameters control the metal angle of the trailing edge, and the deviation between the exit flow angle and the metal angle is small for cascades, one would expect them to have a strong influence on the steady lift.

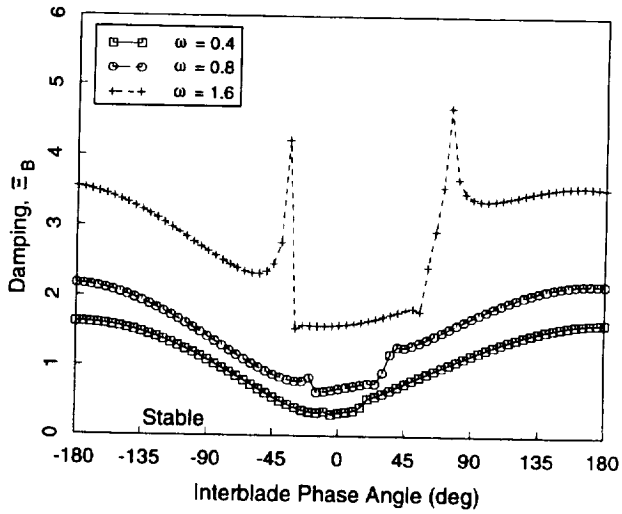

Figure 4: Aerodynamic damping of cascade of NACA 5506 airfoils vibrating in plunge at frequencies of 0.4, 0.8, and 1.6 for a range of interblade phase angles.

Unsteady Flow Through a Compressor

Having computed the steady flow through the cascade, we next consider the unsteady flow due to plunging and torsional vibration of the airfoils. Figure 4 shows the aerodynamic damping Ξ_B of the cascade vibrating in plunge at three reduced frequencies and for a range of interblade phase angles (the aerodynamic damping is proportional to the imaginary part of the unsteady lift). Note that for plunging motion, the system is stable, that is, the aerodynamic damping is positive for all interblade phase angles. However, the aerodynamic damping is generally less for low reduced frequencies (high reduced velocities). The pronounced peaks in the damping curves correspond to acoustic resonance, the point at which acoustic duct modes are "cut-on."

Figure 5 shows the aerodynamic damping Ξ_T for the case where the airfoils vibrate in pitch about their midchords (the damping is proportional to the imaginary part of the unsteady moment). Again, the cascade is least stable at the low reduced frequencies. In particular, note that the system is unstable ($\Xi_T < 0$) for several interblade phase angles at the lowest reduced frequency ω of 0.4.

Consider the case where the airfoils pitch about their midchords with a reduced frequency ω of 0.4 and an interblade phase angle σ of 60° (this is the least stable interblade phase angle for the reduced frequency ω of 0.4). Figure 6 shows the real and imaginary parts of

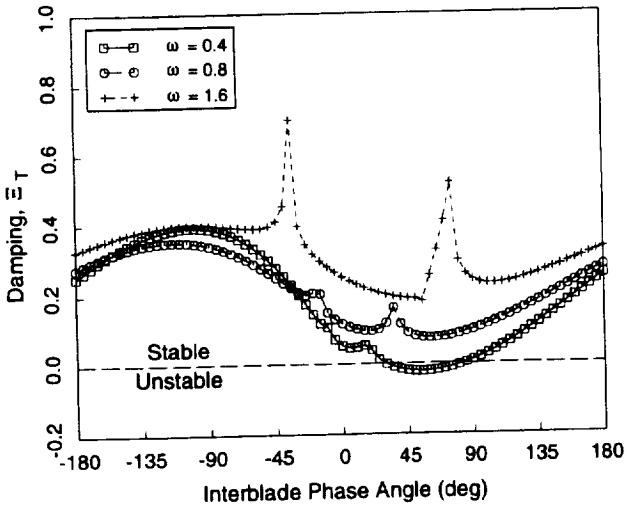

Figure 5: Aerodynamic damping of cascade of NACA 5506 airfoils pitching about their midchords at frequencies of 0.4, 0.8, and 1.6 for a range of interblade phase angles.

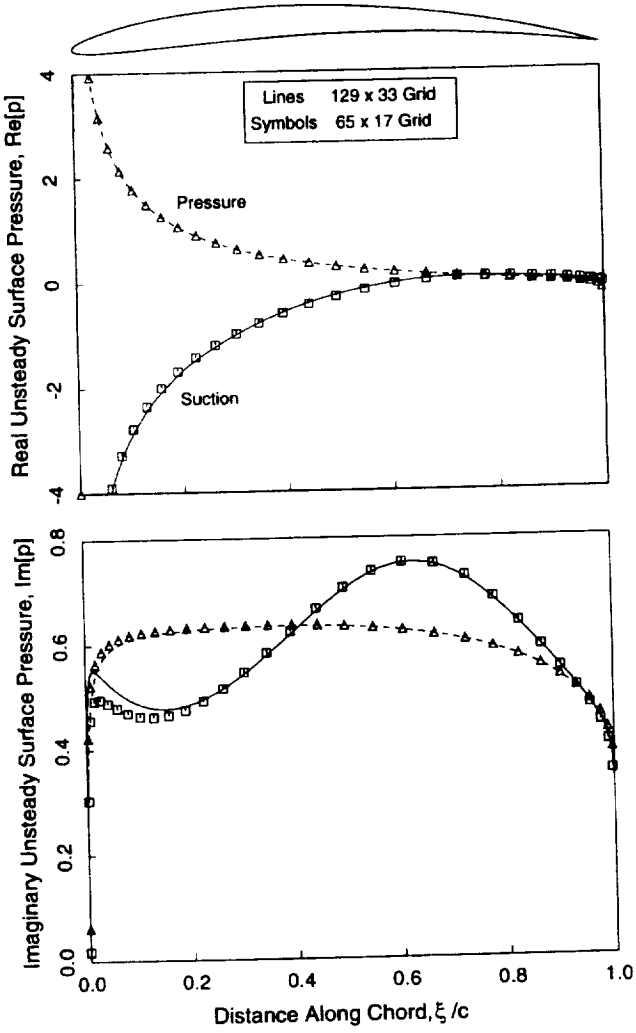

Figure 6: Real and imaginary parts of unsteady surface pressure of NACA 5506 airfoils pitching about their midchords. $\omega = 0.4$, $\sigma = 60°$.

the complex amplitude of the nominal unsteady pressure, p, on the surface of the reference airfoil for two different grid resolutions, a 65×17 node grid and a 129×33 node grid. Note that the imaginary part of the pressure distribution is the part that does work on the vibrating airfoil. For this case, we see that the imaginary part of the pressure difference across the airfoil is generally negative over the front half of the airfoil and positive over the aft half. Thus, since the airfoil pitches about its midchord (positive nose up), the unsteady pressure does positive aerodynamic work (negative aerodynamic damping) on the airfoil over most of the airfoil.

We next compute the sensitivities of the unsteady surface pressure to changes in geometry. Figures 7 and 8 show the real and imaginary parts, respectively, of the sensitivity of the unsteady pressure to small changes in six of seven design variables (the effect of the location of maximum camber is not shown, and the reduced frequency ω is included as a design variable for unsteady flow calculations). All results were computed on a 65×17 node grid. The sensitivities are also compared to a finite difference calculation. Note the excellent agreement between the two solutions indicating that the present method correctly predicts the sensitivities. Also, the imaginary parts of the sensitivities to changes in stagger and reflex have pressure distributions that are fairly large in magnitude and have shapes that would tend to do work on pitching airfoils. That is, the sign of the pressure difference across the airfoil changes at roughly the midchord of the airfoil.

Having computed the sensitivities of the surface pressure to design variables, we can now integrate to obtain the sensitivities of the aerodynamic damping. Table 2 shows the sensitivity of the aerodynamic damping to small changes in the design variables. The column labeled "Unconstrained" gives the sensitivity of the aerodynamic damping to changes in a single parameter. Here Ξ'_T is the sensitivity of the aerodynamic damping due to pitching motions, and Ξ'_B is the sensitivity of the aerodynamic damping due to plunging motion. In both cases, the nominal reduced frequency ω is 0.4. Note that as expected, stagger and reflex have a strong influence on the aerodynamic damping in pitch. Also note that for both pitching and plunging, the sensitivity of the damping to changes in frequency is positive. This is consistent with the results shown in Figures 4 and 5.

The results in the "Unconstrained" column of Table 2, however, can be somewhat misleading since

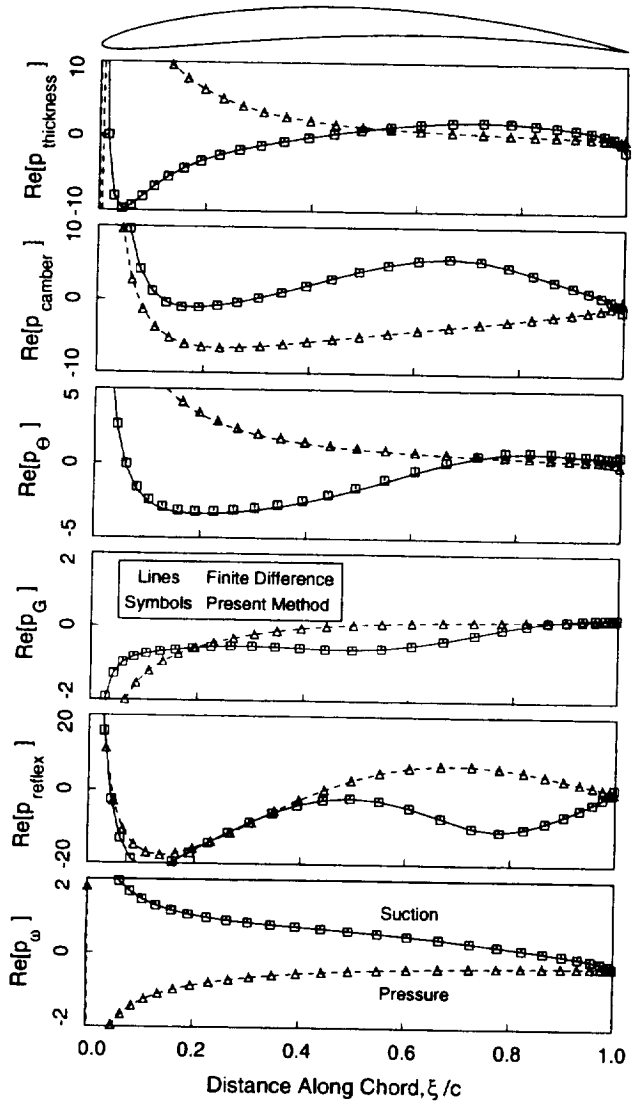

Figure 7: Real part of sensitivity of unsteady surface pressure of NACA 5506 airfoils pitching about their midchords due to perturbations in thickness, camber, stagger, gap, reflex, and frequency. $\omega = 0.4$, $\sigma = 60°$.

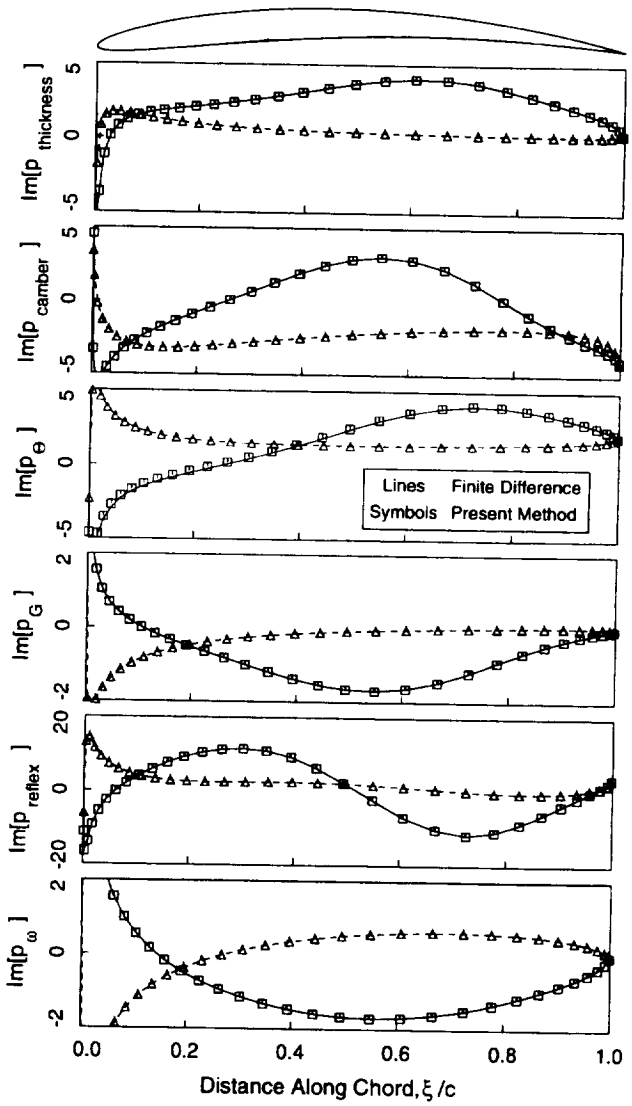

Figure 8: Imaginary part of sensitivity of unsteady surface pressure of NACA 5506 airfoils pitching about their midchords due to perturbations in thickness, camber, stagger, gap, reflex, and frequency. $\omega = 0.4$, $\sigma = 60°$.

changing each design variable independently also changes the steady work done by the cascade and changes the steady incidence at the leading edge of the airfoil. Generally, one would want to leave these quantities unchanged. To avoid this difficulty, it is useful to let two of the design variables "float" so that the steady lift L_y and the leading edge incidence α remains constant. In this study, we allow the stagger angle Θ and the reflex r to float. For example, then, if we vary the gap G, we must vary the stagger angle and reflex such that

$$\frac{\partial L_y}{\partial \Theta}\Theta' + \frac{\partial L_y}{\partial r}r' + \frac{\partial L_y}{\partial G}G' = 0 \qquad (25)$$

$$\frac{\partial \alpha}{\partial \Theta}\Theta' + \frac{\partial \alpha}{\partial r}r' + \frac{\partial \alpha}{\partial G}G' = 0 \qquad (26)$$

Equations (25) and (26) give two equations for the two unknowns Θ' and r' in terms of the perturbation G' and the sensitivities. In Table 2, the column labeled "Constrained" refers to the sensitivities to each variable using this procedure. For both the pitching and plunging cases, it is clear that changing the camber has a very strong effect on the aerodynamic damping. In the pitching case, an increase in camber is destabilizing; in the plunging case, an increase in camber is stabilizing.

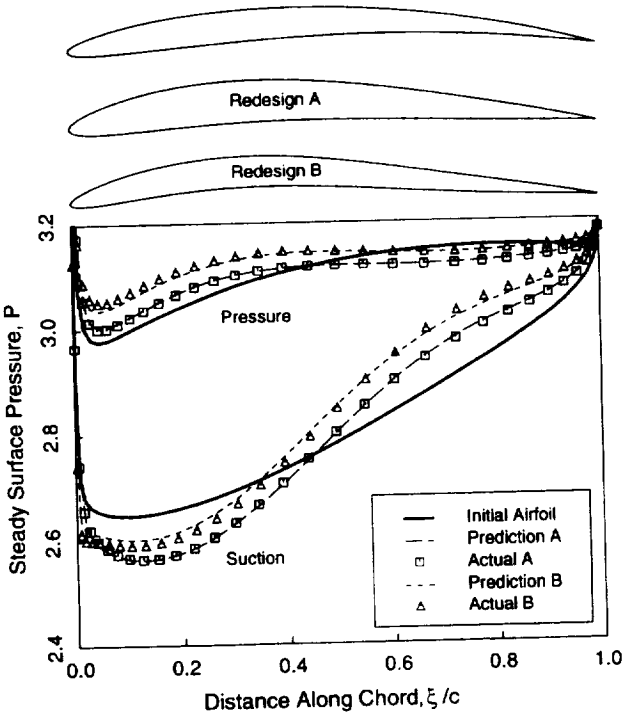

Figure 9: Steady surface pressure of cascade of redesigned airfoils. $M_{-\infty} = 0.5$, $\beta_{-\infty} = 55°$.

Table 2: Sensitivity of aerodynamic damping. The nominal aerodynamic damping in torsion, Ξ_T, *is* -0.0214, *and the damping in plunging,* Ξ_B, *is* 0.8882.

Variable	Unconstrained		Constrained	
	Ξ'_T	Ξ'_B	Ξ'_T	Ξ'_B
Thickness	-0.2208	0.3046	0.1344	-0.1879
Camber	-0.0018	-1.9868	-5.2561	3.3668
Stagger	-0.6672	1.4079	—	—
Gap	0.1723	-0.0237	-0.2564	0.5707
Max. C. Loc.	-0.0383	-0.1143	0.0300	-0.0159
Reflex	0.7362	2.0131	—	—
Frequency	0.4030	1.3337	0.4030	1.3337

Redesign of a Compressor for Aeroelastic Stability

Next, we use the constrained sensitivity analysis to redesign an unstable cascade to make it stable. The nominal cascade has a reduced frequency ω of 0.4 and an interblade phase angle σ of 60°. We note from Table 2 that decreasing the camber has a stabilizing influence on torsional flutter. Thus, for the first redesign (Redesign A), we reduce the camber by 0.004 units. Using the constraint relations above, this requires us to reduce the stagger angle by approximately 1.4° and increase the reflex by 0.0064 units. Although the sensitivity analysis predicts that these changes alone will make the airfoil stable, the sensitivity analysis also predicts a large steady pressure gradient on the suction surface near the leading edge. To smooth out the pressure distribution, we increase the thickness by 0.02 units, which in turn requires us to reduce the stagger by approximately 0.52° and add 0.0014 units of reflex.

For the second redesign (Redesign B), we reduce the gap G by 0.1, Again Table 2 predicts that this change will make the cascade stable, and requires that we reduce the stagger angle by approximately 3.1° and add 0.0261 units of reflex.

Figure 9 shows the computed steady surface pressure on the nominal and redesigned airfoils. Also shown is the pressure predicted by the linear sensitivity analysis. The good agreement between the two indicates that nonlinear geometrical effects are small. Although the steady lift on the airfoil in the y-direction has only slightly changed, the pressure distribution has changed significantly. Note that the pressure gradient on the suction surface is larger for both redesigned airfoils. Both redesigns are therefore likely to increase somewhat the aerodynamic losses of the cascade.

Figure 10 shows the real and imaginary parts of the unsteady pressure on the surface of the redesigned airfoils. Although the real part of the pressure distribution remains largely unchanged, the imaginary part shows significant changes, particularly on the suction surface. Note that the agreement between the sensitivity analysis prediction and the actual pressure distribution, while not quite as good as in the steady case, is still remarkably good. The actual damping of the Redesign A cascade is 0.0086, indicating that the new cascade is stable. The damping of the Redesign B cascade is 0.0030, so this cascade is also stable.

Figure 11 shows the aerodynamic damping of the redesigned airfoils for a reduced frequency ω of 0.4 for a range of interblade phase angles σ. The five lines in the figure correspond to the original nominal damping, the damping of the redesigned airfoils predicted by the sensitivity analysis, and the actual damping of the redesigned airfoils. Note that both redesigned airfoils are stable for all interblade phase angles. In addition, the sensitivity analysis prediction gives excellent estimates of the actual damping of the redesigned airfoils.

Computational Efficiency

Finally, a note about computational times. Table 3 shows the CPU time required to perform various calculations using the present method on a Silicon Graphics Indigo R4000 workstation. All calculations were performed using a 129×33 node computational grid. The steady sensitivity analysis requires only a fraction of the CPU time necessary to perform a single nominal steady calculation. For the seven design variables considered here, the unsteady sensitivity analysis required about six times the CPU time as a single nominal unsteady

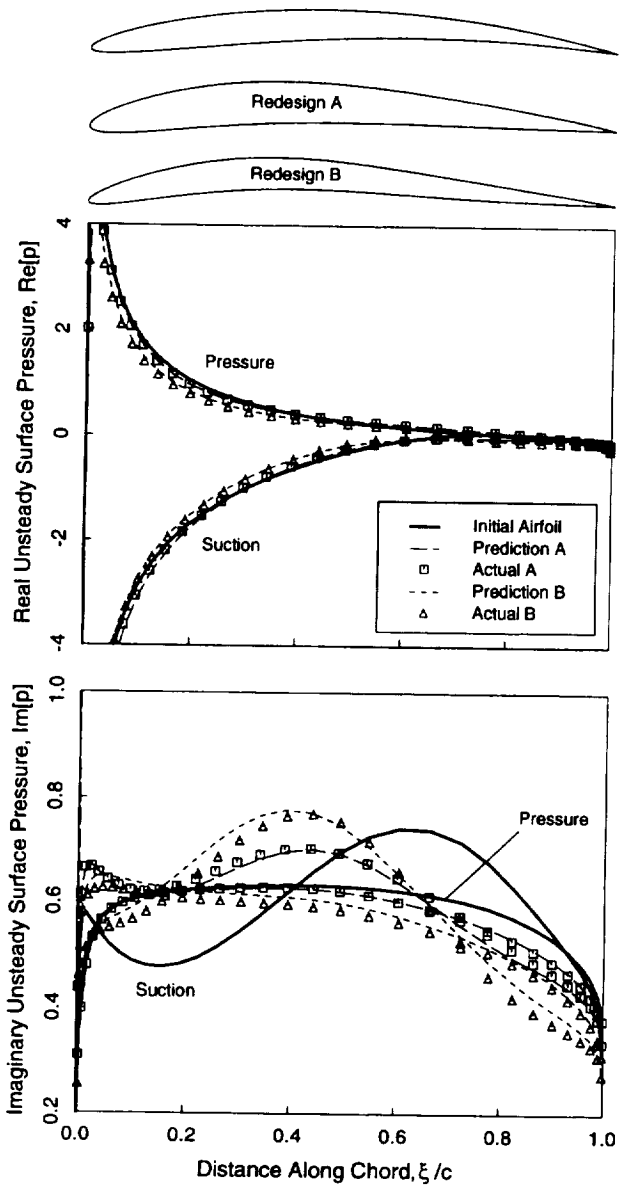

Figure 10: Real and imaginary parts of unsteady surface pressure of redesigned airfoils pitching about their midchords. $\omega = 0.4$, $\sigma = 60°$.

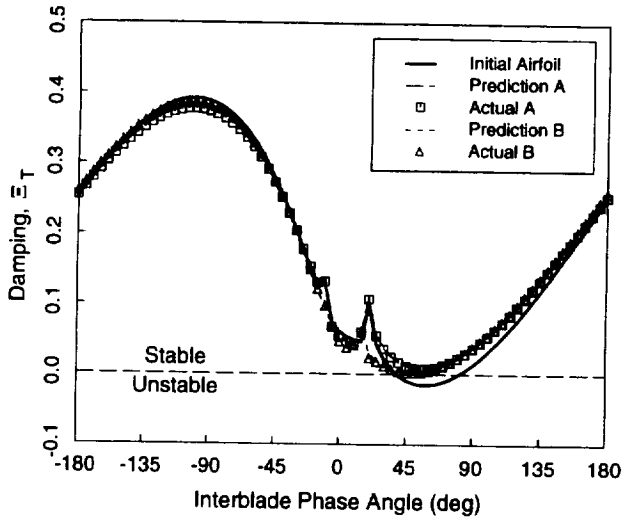

Figure 11: Aerodynamic damping of cascade of redesigned airfoils pitching about their midchords at a frequency of 0.4 for a range of interblade phase angles.

Table 3: Computational times for present method using 129 × 33 node grid.

Procedure	CPU Time (sec)
Present Method	
Nominal Steady	23.6
Nominal Unsteady	7.2
Steady Sensitivity (6 var)	4.7
Unsteady Sensitivity (7 var)	42.5
Finite Difference	
Steady Sensitivity (6 var)	283.6
Unsteady Sensitivity (7 var)	100.4

calculation, but only about half of what was required for a finite difference sensitivity analysis. Furthermore, the present sensitivity analysis, unlike the finite difference analysis, is not susceptible to truncation and round-off errors.

Conclusions

In this paper, a new method for calculating the sensitivity of steady and unsteady flows in cascades to small changes in airfoil and cascade geometry is presented. First, the steady and small disturbance unsteady flow through the cascade is modeled using the steady and linearized versions of the full potential equation. A variational finite element technique is used to discretize the steady and small disturbance unsteady potential equations. Newton iteration is used to solve the steady equations with LU decomposition used at each step; the small disturbance equations are linear and solved with a single LU decomposition.

The sensitivities of the steady and unsteady flow fields to changes in geometry are computed by perturbing the finite element scheme about the nominal solution. The resulting matrix equations for the steady and unsteady sensitivity solutions have similar forms to the nominal flow equations. In fact the matrix equations to be solved have matrices that are identical to those in the nominal flow solvers. Thus, once the nominal flows

have been computed, the sensitivity analysis requires very little additional computer time. Furthermore, the method is general and can also be applied to finite difference and finite volume calculations so long as the nominal flow solvers use LU decomposition.

Finally, we have demonstrated that the sensitivity analysis may be used to guide in the aeroelastic redesign of airfoils. In the example presented in the paper, a cascade that was aeroelastically unstable in torsion was redesigned to be aeroelastically stable.

Acknowledgments

This work was supported by NASA Lewis Research Center, NASA Grant NAG3-1433, with Dr. Daniel Hoyniak serving as technical monitor.

References

[1] Verdon, J. M., "Linearized Unsteady Aerodynamic Theory," Chapter 2 in AGARD Manual on Aeroelasticity in Axial-Flow Turbomachines,Unsteady Turbomachinery Aerodynamics, Vol. 1, M. F. Platzer and F. O. Carta (eds.), AGARD-AG-298, March 1987.

[2] Whitehead, D. S., "Classical Two-Dimensional Methods," Chapter 3 in AGARD Manual on Aeroelasticity in Axial-Flow Turbomachines, Unsteady Turbomachinery Aerodynamics, Vol. 1, M. F. Platzer and F. O. Carta (eds.), AGARD-AG-298, March 1987.

[3] Hall, K. C. and Verdon, J. M., "Gust Response Analysis for Cascades Operating in Nonuniform Mean Flows," *AIAA Journal*, Vol. 29, No. 9, 1991, pp. 1463-1471.

[4] Fang, J. and Atassi, H. M., "Numerical Solutions for Unsteady Subsonic Vortical Flows Around Loaded Cascades", *Transactions of the ASME: Journal of Turbomachinery*, Vol. 115, No. 4, 1993, pp. 810-816.

[5] Hall, K. C. and Clark, W. S., "Linearized Euler Prediction of Unsteady Aerodynamic Loads in Cascades", *AIAA Journal*, Vol. 31, No. 3, 1993, pp. 540-550.

[6] Holmes, D. G. and Chuang, H. A., "2D Linearized Harmonic Euler Flow Analysis for Flutter and Forced Response," *Unsteady Aerodynamics, Aeroacoustics, and Aeroelasticity of Turbomachines and Propellers*, H. M. Atassi (ed.), Springer-Verlag, New York, 1993.

[7] Kahl, G. and Klose, A., "Time Linearized Euler Calculations for Unsteady Quasi-3D Cascade Flows," *Unsteady Aerodynamics, Aeroacoustics, and Aeroelasticity of Turbomachines and Propellers*, H. M. Atassi (ed.), Springer-Verlag, New York, 1993.

[8] Hall, K. C. and Lorence, C. B., "Calculation of Three-Dimensional Unsteady Flows in Turbomachinery Using the Linearized Harmonic Euler Equations," *Transactions of the ASME: Journal of Turbomachinery*, Vol. 115, No. 4, 1993, pp. 800-809.

[9] Lighthill, M. J., "A New Method of Two-Dimensional Aerodynamic Design," Aeronautical Research Council, Reports and Memorandum 2112, 1945.

[10] Giles, M. B. and Drela, M., "Two-Dimensional Transonic Aerodynamic Design Method," *AIAA Journal*, Vol. 25, 1987, pp. 1199-1206.

[11] Bock, K. W., "Aerodynamic Design by Optimization," in AGARD, Computational Methods for Aerodynamic Design (Inverse) and Optimization, AGARD-CP-463.

[12] Jameson, A., "Aerodynamic Design via Control Theory," NASA Contract Report CR-181749.

[13] Ganguli, R. and Chopra, I., "Aeroelastic Optimization of an Advanced Geometry Helicopter Rotor," Presented at the AIAA/ASME/ASCE/AHS/ASC Structures, Structural Dynamics and Materials Conference, Dallas, TX, April 24-27, 1992. AIAA Paper 92-2360-CP.

[14] Dodd, A. J., Kadrinka, K. E., Loikkanen, M. J., Rommel, B. A., Sikes, G. D., Strong, R. C., and Tzong, T. J., "Aeroelastic Design Optimization Program," *Journal of Aircraft*, Vol. 27, No. 12, 1990, pp. 1028-1036.

[15] Crawley, E. F., and Hall, K. C., "Optimization and Mechanisms of Mistuning in Cascades," *Transactions of the ASME: Journal of Engineering for Gas Turbines and Power*, Vol. 107, No. 2, 1985, pp. 418-426.

[16] Adelman, H. M. and Haftka, R. T., "Sensitivity Analysis of Discrete Structural Systems," *AIAA Journal*, Vol. 24, No. 5, 1986, pp. 823-832.

[17] Haug, E. J., Choi, K. K., and Komkov, V., *Design Sensitivity Analysis of Structural Systems*, Academic Press, Orlando, 1986.

[18] Taylor, A. C., III, Hou, G. W., and Korivi, V. M., "Methodology for Calculating Aerodynamic Sensitivity Derivatives," *AIAA Journal*, Vol. 30, No. 10, 1992, pp. 2411-2419.

[19] Baysal, O. and Eleshaky, M. E., "Aerodynamic Design Optimization Using Sensitivity Analysis and Computational Fluid Dynamics," *AIAA Journal*, Vol. 30, No. 3, 1992, pp. 718-725.

[20] Sadrehaghighi, I., Smith, R. E., and Tiwari, S. N., "Grid and Design Variables Sensitivity Analyses for NACA Four-Digit Wing-Sections," Presented at the AIAA 31st Aerospace Sciences Meeting, Reno, NV, January 11-14, 1993. AIAA Paper 93-0195.

[21] Murthy, D. B. and Kaza, K. R. V., "Semianalytical Technique for Sensitivity Analysis of Unsteady Aerodynamic Computations," *Journal of Aircraft*, Vol. 28, No. 8, 1991, pp. 481-488.

[22] Hall, K. C., "Deforming Grid Variational Principle for Unsteady Small Disturbance Flows in Cascades," *AIAA Journal*, Vol. 31, No. 5, 1993, pp. 891-900.

[23] Verdon, J. M., "The Unsteady Flow in the Far Field of an Isolated Blade Row," *Journal of Fluids and Structures*, Vol. 3, 1989, pp. 123-149.

[24] Bateman, H., "Irrotational Motion of a Compressible Fluid," Proc. National Academy of Sciences, Vol. 16, 1930, p. 816.